FULL PAPER

BJC

British Journal of Cancer (2018) 118, 366–377 | doi: 10.1038/bjc.2017.421

Keywords: MTOR; pancreatic cancer; therapeutic resistance

MTOR inhibitor-based combination therapies for pancreatic cancer

Zonera Hassan[1], Christian Schneeweis[1], Matthias Wirth[2], Christian Veltkamp[1], Zahra Dantes[1], Benedikt Feuerecker[3,4], Güralp O Ceyhan[5], Shirley K Knauer[6], Wilko Weichert[7], Roland M Schmid[1], Roland Stauber[8], Alexander Arlt[9], Oliver H Krämer[10], Roland Rad[1,4], Maximilian Reichert[1,11], Dieter Saur[1,4] and Günter Schneider*[,1,4]

[1]Medical Clinic and Polyclinic II, Klinikum rechts der Isar, Technical University Munich, 81675 München, Germany; [2]Institute of Pathology, Heinrich-Heine University and University Hospital Düsseldorf, 40225 Düsseldorf, Germany; [3]Department of Nuclear Medicine, Klinikum rechts der Isar, Technical University Munich, 81675 München, Germany; [4]German Cancer Research Center (DKFZ) and German Cancer Consortium (DKTK), 69120 Heidelberg, Germany; [5]Department of Surgery, Klinikum rechts der Isar, Technical University of Munich, 81675 München, Germany; [6]Molecular Biology, Centre for Medical Biotechnology (ZMB), University Duisburg-Essen, 45141 Essen, Germany; [7]Institute of Pathology, Technische Universität München, 81675 München, Germany; [8]Molecular and Cellular Oncology/ENT, University Medical Center Mainz, Langenbeckstrasse 1, Mainz 55131, Germany; [9]Laboratory of Molecular Gastroenterology and Hepatology, 1st Department of Internal Medicine, University Hospital Schleswig-Holstein, Kiel, Germany; [10]Department of Toxicology, University of Mainz Medical Center, Mainz 55131, Germany and [11]Division of Gastroenterology and Abramson Cancer Center, Perelman School of Medicine, University of Pennsylvania, Philadelphia, PA 19104, USA

Background: Although the mechanistic target of rapamycin (MTOR) kinase, included in the mTORC1 and mTORC2 signalling hubs, has been demonstrated to be active in a significant fraction of patients with pancreatic ductal adenocarcinoma (PDAC), the value of the kinase as a therapeutic target needs further clarification.

Methods: We used *Mtor* floxed mice to analyse the function of the kinase in context of the pancreas at the genetic level. Using a dual-recombinase system, which is based on the flippase-FRT (Flp-FRT) and Cre-loxP recombination technologies, we generated a novel cellular model, allowing the genetic analysis of MTOR functions in tumour maintenance. Cross-species validation and pharmacological intervention studies were used to recapitulate genetic data in human models, including primary human 3D PDAC cultures.

Results: Genetic deletion of the *Mtor* gene in the pancreas results in exocrine and endocrine insufficiency. In established murine PDAC cells, MTOR is linked to metabolic pathways and maintains the glucose uptake and growth. Importantly, blocking MTOR genetically as well as pharmacologically results in adaptive rewiring of oncogenic signalling with activation of canonical extracellular signal-regulated kinase and phosphoinositide 3-kinase-AKT pathways. We provide evidence that interfering with such adaptive signalling in murine and human PDAC models is important in a subgroup.

Conclusions: Our data suggest developing dual MTORC1/TORC2 inhibitor-based therapies for subtype-specific intervention.

*Correspondence: Dr G Schneider; E-mail: guenter.schneider@tum.de

Received 28 June 2017; revised 25 October 2017; accepted 26 October 2017; published online 2 January 2018

Understanding the complexity of context-specific oncogenic signalling, including feedforward and feedbackward loops and the adaption of signalling upon targeted intervention is a major goal to develop precision therapies (Schneider *et al*, 2017). Over 90% of pancreatic ductal adenocarcinoma (PDAC) patients harbour oncogenic KRAS mutations. Mutated KRAS initiates a complex and context-specific signalling, including canonical mitogen-activated protein kinase kinase (MEK)-extracellular signal-regulated kinase (ERK) or phosphoinositide 3-kinase (PI3K)-3-phosphoinositide-dependent protein kinase (PDK1) pathways (Schneeweis *et al*, 2016). Indeed, the PI3K-PDK1 signalling pathway is a KRAS effector in the pancreas. Genetic deletion of the PI3K subunit *p110α* (Baer *et al*, 2014; Wu *et al*, 2014) or *Pdk1* (Eser *et al*, 2013; Schonhuber *et al*, 2014) blocks the formation of preneoplastic lesions as well as the development of invasive cancers in genetically engineered mouse models (GEMMs). Moreover, the H1047R hotspot mutant of *p110α* drives carcinogenesis in the pancreas (Eser *et al*, 2013; Payne *et al*, 2015). At the therapeutic level, it has been demonstrated that inhibition of the PI3K pathway leads to growth inhibition and temporal tumour stasis in PDAC GEMMs as well as patient-derived orthotopic xenotransplant models (Cao *et al*, 2009; Eser *et al*, 2013; Junttila *et al*, 2015; Payne *et al*, 2015).

The Ser/Thr kinase mechanistic target of rapamycin (MTOR) is an important downstream target of the PI3K signalling pathway (Saxton and Sabatini, 2017). Mechanistic target of rapamycin is included in the two protein complexes mTORC1 and mTORC2. The mTORC1 complex also contains regulatory-associated protein of MTOR (RAPTOR) and mammalian lethal with SEC thirteen 8 (mLST8), whereas the mTORC2 complex is characterised by the presence of rapamycin-insensitive companion of MTOR (RICTOR), SAPK-interacting 1 and mLST8. mTORC1, the activity of which is controlled by growth factors, cellular energy balance and nutrient supply, phosphorylates downstream targets including ribosomal S6 kinase and eIF4E-binding protein 1 (4E-BP1) to promote protein, nucleotide or lipid synthesis. Growth factors stimulate mTORC2 to phosphorylate certain kinases of the AGC family. Pancreatic ductal adenocarcinomas carry phosphorylation of Ser2448 of MTOR (Kennedy *et al*, 2011; Kong *et al*, 2016), which marks the activation of this signalling node. In line with activation in a significant fraction of PDAC patients, the MTOR kinase integrates the signal of the two main driver pathways: the MEK-ERK (Kong *et al*, 2016) and the PI3K pathways (Morran *et al*, 2014). Together, such data argue that MTOR is a relevant node and therapeutic target in PDAC.

We conducted this study to further clarify the role of MTOR as a therapeutic target in PDAC. To fulfil this task, we developed a new model to genetically inactivate *Mtor* in established murine PDAC cells. We show that MTOR is a regulator of metabolic programmes and growth in PDAC, we describe adaptive rewiring of oncogenic signalling in response to the MTOR blockade and point to opportunities for dual MTOR inhibitor-based combination therapies by addressing adaptive rewiring programmes.

MATERIALS AND METHODS

Compounds. The MK-2206 was purchased from Selleckchem (Eching, Germany), PD-325901 and camptothecin from Sigma (Munich, Germany), GDC-0941, bortezomib, and INK-128 from LC Laboratories (Woburn, MA, USA). AZD2014 was purchased from BioVision (Milpitas, CA, USA) and MRT67307 from Cayman Chemicals/Biomol (Hamburg, Germany). 4-Hydroxytamoxifen was purchased from Sigma.

Mouse lines and blood glucose. The conditional ready *Mtor* mouse line (*Mtor*$^{tm1a(EUCOMM)Wtsi}$) was generated by EUCOMM and obtained via EMMA. The mouse line was recently used by Beirowski *et al* (2014). The line was interbred with *Rosa26-Flpo* mice (Raymond and Soriano, 2010) to generate *Mtor* floxed mice. The *FSF-Kras*^{G12D} (Schonhuber *et al*, 2014), *Pdx1-Flp* (Schonhuber *et al*, 2014), *FSF-R26*$^{CAG\text{-}CreERT2}$ (Schonhuber *et al*, 2014), *Ptf1a*^{Cre} (Eser *et al*, 2013), *LSL-Kras*^{G12D} (5) and *R26*$^{mT/mG}$ (Muzumdar *et al*, 2007) lines have been described. Genotyping primers have been described (Eser *et al*, 2013; Schonhuber *et al*, 2014; Diersch *et al*, 2015) or are depicted in Supplementary Materials and Methods (SM&M). Animals were on a mixed *C57Bl/6;129S6/SvEv* genetic background. *KC;Mtor*$^{lox/lox}$ and *Ptf1a*^{Cre}*;Mtor*$^{lox/lox}$ mice were fed with a chow diet substituted with 10 g kg^{-1} Pancrex-Vet (Ssniff Spezialdiäten GmbH, Soest, Germany) throughout life. For monitoring of blood glucose, a glucometer (Abbott Laboratories, Wiesbaden, Germany) was used and operated according to the manufacturer's instructions. Glucose was measured under normal feeding conditions. Animal studies were conducted in compliance with European guidelines for the care and use of laboratory animals and were approved by the Institutional Animal Care and Use Committees of the Technische Universität München and Regierung von Oberbayern.

Cell lines. Murine pancreatic cancer cell lines were established from genetically engineered *Kras*^{G12D}-driven mouse models and cultivated as described (von Burstin *et al*, 2009). All cell lines were cultured in DMEM medium (Sigma-Aldrich Chemie GmbH, Munich, Germany) or RPMI supplemented with GlutaMax (Gibco by Life Technologies, Darmstadt, Germany) containing 10% fetal calf serum (FCS) (Merck Millipore/Biochrom, Berlin, Germany) supplemented with 1% (w v^{-1}) penicillin/streptomycin (Life Technologies). Identity of the murine pancreatic cancer cell lines was verified using genotyping PCR. Human cell lines were authenticated by single-nucleotide polymorphism (SNP) profiling conducted by Multiplexion GmbH (Heidelberg, Germany). Cell lines were tested for Mycoplasma contamination by a PCR-based method described by Ossewaarde *et al* (1996). To genetically manipulate *Mtor* expression, a cell line with the following genotype was generated: *Pdx1-Flp;FSF-Kras*^{G12D}*;FSF-R26*$^{CAG\text{-}CreERT2}$*;R26*$^{mT/mG}$*;mTor*$^{\Delta E3/lox}$ (cell line: PPT4-ZH363-*Mtor*$^{\Delta E3/lox}$). As a control for Cre and tamoxifen toxicity, the PPT-c1674 (*Pdx1-Flp;FSF-Kras*^{G12D}*;FSF-R26*$^{CAG\text{-}CreERT2}$*;R26*$^{mT/mG}$) PDAC cell line was used. Tomato expressing PPT4-ZH363-*Mtor*$^{\Delta E3/lox}$ cells were FACS sorted as described (Wirth *et al*, 2014) to assure epithelial identity and used for all subsequent experiments. To activate Cre^{ERT2}, PDAC cells were treated with vehicle (ethanol) or 600 nM 4-hydroxytamoxifen (4-OHT) for 8 days. Afterwards, cells were used for individual assays.

Primary human PDAC 3D culture. PDAC tissues (B20: pT3, pN1, G3; B25: pT3, pN1, G2) were obtained from patients undergoing surgical resection at the Department of Surgery of the Technical University of Munich. All tissues were confirmed to be PDAC by pathological examination. Human primary PDAC 3D cultures experiments were in accordance with the Declaration of Helsinki, were approved by the ethical committee of the Technical University of Munich and written informed consent from the patients for research use of the cancer tissue was obtained before the investigation of the specimens. Generation and expansion of primary PDAC 3D cultures was performed as described (Boj *et al*, 2015). Furthermore, isolation, culturing and drug treatment is described in SM&M.

Viability assay, cell-cycle FACS, GI_{50} calculation and synergy score. Viability was measured using MTT assays as described in SM&M. For cell-cycle FACS analysis, cells were detached by trypsinisation and washed two times in PBS followed by fixation in 1 ml cold 70% EtOH. After 24 h, EtOH was removed and cells were washed in PBS. RNA was digested by adding RNAse (Sigma) (final

concentration 0.5 $\mu g\,ml^{-1}$) for 1 h. Cells were stained by adding 50 μl propidium iodide (PI) (50 $\mu g\,ml^{-1}$) (Sigma) and analysed using FACS Gallios (Beckman Coulter, Krefeld, Germany). Data were analysed by using the FlowJo software (FlowJo, LLC, Ashland, OR, USA). The growth inhibitory 50% (GI_{50}) concentration of the inhibitors was calculated with GraphPad Prism6 (GraphPad Software, San Diego, CA, USA) using a nonlinear regression model (log inhibitor *vs* response (three parameters)). The synergy score (SC) was calculated according to $SC = \log 10(GI_{50control}/GI_{50combination})$.

Clonogenic assay. Two thousand dispersed cells were plated in 6-well plates, and grown for 14 days in growth medium containing 10% FCS supplemented with 1% ($w\,v^{-1}$) penicillin–streptomycin. Afterwards cells were fixed with methanol, stained with Giemsa solution (1 : 20 dilution) (Sigma) and scanned for visualisation.

Cell lysis and western blot. To prepare whole-cell extracts (WCEs), immunoprecipitation buffer (50 mM HEPES, 150 mM NaCl, 1 mM EDTA, 0.5% NP-40, 10% glycerol) supplemented with protease and phosphatase inhibitors (cOmplete, EDTA-free Protease Inhibitor Cocktail (Roche Diagnostics, Mannheim, Germany) and Phosphatase-Inhibitor-Mix I (Serva, Heidelberg, Germany)) was used. Whole-cell extracts were normalised for protein and heated at 95 °C for 5 min in protein loading buffer (45.6 mM Tris-HCl (pH 6.8), 2% SDS, 10% glycerol, 1% β-mercaptoethanol, 0.01% bromophenol blue). Western blotting and primary/secondary antibodies are described in SM&M.

Quantitative reverse-transcriptase PCR. Total RNA was isolated from PDAC cell lines using the RNeasy Kit (Qiagen, Hilden, Germany) following the manufacturer's instructions. Quantitative mRNA analysis was performed using real-time PCR analysis system (TaqMan, PE StepOnePlus, Real-Time PCR System; Applied Biosystems Inc., Carlsbad, CA, USA) by using SYBR Green Master Mix (Applied Biosystems/ThermoFisher) as fluorescent DNA binding dye. Primers can be found in SM&M. Data analysis was carried out with Stepone software (Applied Biosystem) according to the ΔΔCt method.

Histochemistry and immunohistochemistry. For histopathological analysis, murine tissues were fixed in 4% formaldehyde (Carl Roth, Karlsruhe, Germany), embedded in paraffin and sectioned (2 μm thick). Tissues were stained with haematoxylin and eosin as described (Diersch *et al*, 2013). For immunohistochemistry, see SM&M.

F-18-FDG uptake assay. A total of 1×10^5 murine PDAC cells were used for quantification of F-18-FDG uptake as described in SM&M.

RNA-Seq analysis, visualisation, cluster analysis, GSEA, Hallmark, GO-Term and KEGG analysis. mRNA was extracted as described above and quality was controlled by densitometry using agarose gel electrophoresis. RNA-sequencing (RNA-Seq) was carried out by the genomics and proteomics core facility of the DKFZ (Heidelberg, Germany; ~25M reads/sample (single-end reads); Illumina HiSeq 2000, San Diego, CA, USA). Next-generation sequencing data were analysed using the Galaxy platform (Goecks *et al*, 2013; Afgan *et al*, 2016). The detailed analysis is described in SM&M. RNA-Seq data were deposited in the NCBI Gene Expression Omnibus with the Accession ID: GSE98860. Enrichment analysis was performed using the gene set enrichment analysis (GSEA) tool (gene set matrix composed files: h.all.v6.0.symbols.gmt) (Subramanian *et al*, 2005). The false discovery rate (FDR) *q*-values, nominal *P*-values and family-wise error rate (FWER) *P*-values were depicted in the figures. Gene ontology (GO)-Term and KEGG analysis of genes downregulated ($\log 2FC \leqslant -0.58$) upon deletion of *Mtor* was conducted using the Database for Annotation, Visualisation and Integrated Discovery (DAVID) (Huang da *et al*, 2009). Terms and pathways with a Benjamini-corrected *P*-value <0.05 were depicted. Heat maps were generated by Heatmapper (Babicki *et al*, 2016) or ClustVis (Metsalu and Vilo, 2015). Human PDAC RNA-Seq data were from Bailey *et al* (2016). Cluster and expression analyses of these data are described in SM&M. TCGA PDAC transcriptome data sets as well as clinical data of the TCGA PDAC dataset were accessed via the UCSC cancer genomics browser (https://genome-cancer.ucsc.edu). Survival data was extracted and assigned to the *LDHA* mRNA expression profile. Low *LDHA* mRNA expression was defined as expression <25th percentile; high *LDHA* mRNA expression was defined as expression >75th percentile; intermediate expression: remaining PDACs.

Statistical methods. Analysis of variance or two-sided Student's *t*-test was used to investigate statistical significance, as indicated. Kaplan–Meier curve were analysed by Log-rank test. *P*-values were calculated with GraphPad Prism6 (GraphPad Software) and corrected according to Bonferroni for multiple testing. Unless otherwise illustrated, all data were determined from at least three independent experiments and presented as mean and standard error of the mean (s.e.m.).

RESULTS

Deletion of *Mtor* in the pancreas induces endocrine and exocrine insufficiency in the context of oncogenic Kras. Recent evidence suggests that dual mTORC1/TORC2 inhibition is a therapeutic option for PDAC (Driscoll *et al*, 2016). To further substantiate this note, we used floxed *Mtor* mice. *Mtor* alleles are specifically deleted in the pancreas of $Ptf1a^{Cre/+}$;$LSL\text{-}Kras^{G12D/+}$;$Mtor^{lox/lox}$ (*KC;Mtor*$^{lox/lox}$) mice (Supplementary Figure 1A). The median survival of heterozygous $Ptf1a^{Cre/+}$;$LSL\text{-}Kras^{G12D/+}$;$Mtor^{lox/+}$ (*KC;Mtor*$^{lox/+}$) mice (Supplementary Figure 1B) was similar to our cohort of $Ptf1a^{Cre}$;$LSL\text{-}Kras^{G12D/+}$ (*KC*) mice (Diersch *et al*, 2013). In contrast, the median survival of homozygous *KC;Mtor*$^{lox/lox}$ mice was distinctly reduced (Supplementary Figure 1B). Compared to controls, the body weight of *KC;Mtor*$^{lox/lox}$ mice was reduced (Supplementary Figure 1C) and the pancreas was macroscopically atrophic (Supplementary Figure 1D). Decreased eosin staining is evident in the disorganised acinar apparatus of *KC;Mtor*$^{lox/lox}$ mice (Supplementary Figure 2A). Acinar structures express amylase (Supplementary Figure 2B). Acinar to ductal metaplasia and low-grade pancreatic intraepithelial neoplasias develop in *KC;Mtor*$^{lox/lox}$ mice and desmoplasia is observed (Supplementary Figures 2A and B). Epithelial lesions stain positive for KRT19 (Supplementary Figure 2B). When substituted with pancreatic enzymes, *KC;Mtor*$^{lox/lox}$ mice gained weight (Supplementary Figure 2C).

Immunohistochemistry demonstrates impaired phosphorylation of eukaryotic translation initiation factor 4E-BP1 (Supplementary Figure 3A) and the S6 ribosomal protein (S6) (Supplementary Figure 3B) in the epithelial compartment. Both phosphorylation events are conducted by MTOR, corroborating the note that the gene is deleted in the epithelial compartment. Islets of Langerhans are present in *KC;Mtor*$^{lox/lox}$ mice, but show impaired staining for insulin (Supplementary Figure 3C). Coincidently, increased blood glucose levels were detected and *KC;Mtor*$^{lox/lox}$ mice, which develop diabetes mellitus at 11 weeks of age (Supplementary Figure 3D). A hypothropic pancreas embedded in adipose tissue was also detected in one analysed $Ptf1a^{Cre}$;$Mtor^{lox/lox}$ mouse (Supplementary Figure 4A). This phenotype is connected to an impaired weight gain (Supplementary Figure 4B). Again, Islets of Langerhans are present in the $Ptf1a^{Cre}$;$Mtor^{lox/lox}$ mouse (Supplementary Figure 4A), but increased blood glucose was measured in this mouse (Supplementary Figure 4C). Taken

together, these data suggest that the *Mtor* gene is needed for the functions of the endocrine and exocrine pancreas.

Generation of a novel model allowing genetic inactivation of MTOR. Since the generation of *Mtor* knockout PDAC cells is not possible in the conventional GEMM, we used a novel dual-recombinase system to generate a cellular model allowing the genetic inactivation of *Mtor* in established cancer cells (Schonhuber *et al*, 2014) to investigate the function of the kinase in tumour maintenance. In this model, the Flp-FRT recombination technology induces the expression of $KRAS^{G12D}$ and a tamoxifen-activatable Cre (Cre^{ERT2}) in the pancreatic epithelium (Schonhuber *et al*, 2014). Therefore, floxed genes can be manipulated in established PDAC cells by tamoxifen treatment (Figure 1A). To minimise the probability of escape from *Mtor* deletion and to allow efficient genetic inactivation of the pathway, we established a murine PDAC cell line with already one deleted *Mtor* allele (PPT4-ZH363-$Mtor^{\Delta E3/lox}$ cells). The presence of a reporter allele allows monitoring Cre-mediated recombination in PPT4-ZH363-$Mtor^{\Delta E3/lox}$ cells upon treatment with 4-OHT (Figure 1B).

Recombination PCR demonstrates that the remaining *Exon 3* of the *Mtor* gene is excised after the treatment with 4-OHT (Figure 1C). Consistently, RNA-Seq data show deletion of *exon 3* of the gene upon the treatment with 4-OHT (Supplementary Figure 5). To further substantiate the loss of MTOR expression, we tested for mRNA and protein expression. Corresponding to the reduced expression of the *Mtor* mRNA over time (Figure 1D), MTOR protein expression is decreased upon the treatment of cells with 4-OHT (Figure 1E). No significant reduction of MTOR was detected in murine PPT-c1647 cells. These PDAC cell line express Cre^{ERT2} and hence can serve control for 4-OHT and Cre toxicities (Figures 1D and E).

MTOR controls proliferation and clonogenic growth. To demonstrate the functional blockade of MTOR signalling, we conducted western blots with phospho-specific antibodies. As expected, loss of MTOR protein expression leads to impaired phosphorylation of S6 and 4E-BP1 (Figure 2A). Mostly hypophosphorylated 4E-BP1 is expressed in *Mtor*-deleted cells, additionally supporting an efficient inactivation of MTOR signalling (Figure 2A). To demonstrate a therapeutic potential of MTOR,

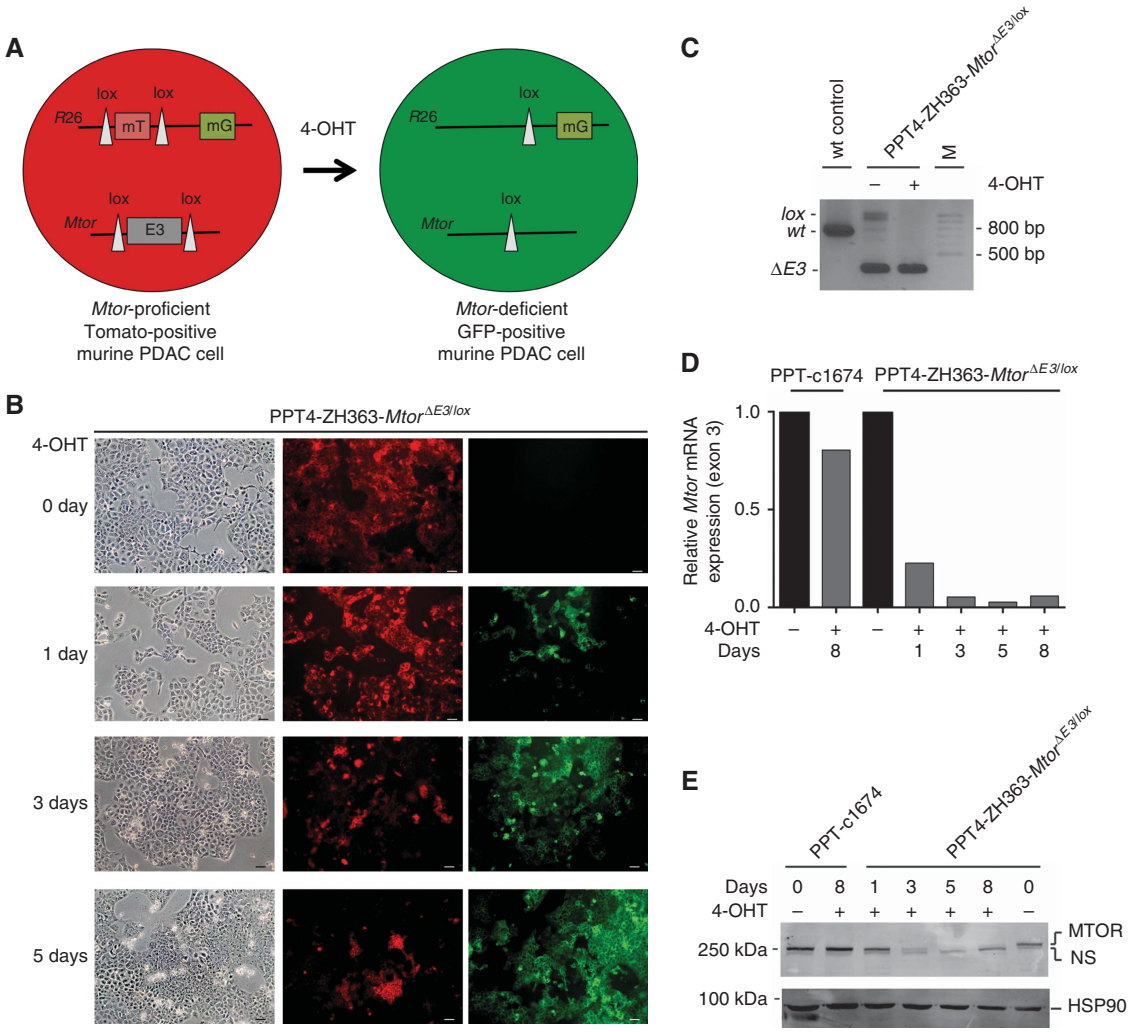

Figure 1. A novel model to genetically inactivate Mtor in PDAC cells. (**A**) Model to inactivate the *Mtor* gene in $Kras^{G12D}$-driven murine PDAC cells. (**B**) Visualisation of 4-OHT-induced recombination events with a double fluorescent floxed tdTomato-EGFP reporter line ($R26^{mT/mG}$). Scale bar, 10 μM. (**C**) Genotyping PCR of the indicated PDAC cells treated with 4-OHT (600 nM, 8 days). *wt*, Wild-type allele; *ΔE3*, exon 3-deleted *Mtor* allele; *lox*, *Mtor* exon 3 floxed allele. (**D**) *Mtor* mRNA expression was determined by quantitative PCR (qPCR) using *beta-actin* mRNA expression as reference ($n = 1$). (**E**) Western blot of MTOR from vehicle- or 4-OHT- (600 nM) treated cells over the indicated time points (heat-shock protein 90 (HSP90): loading control) ($n = 2$).

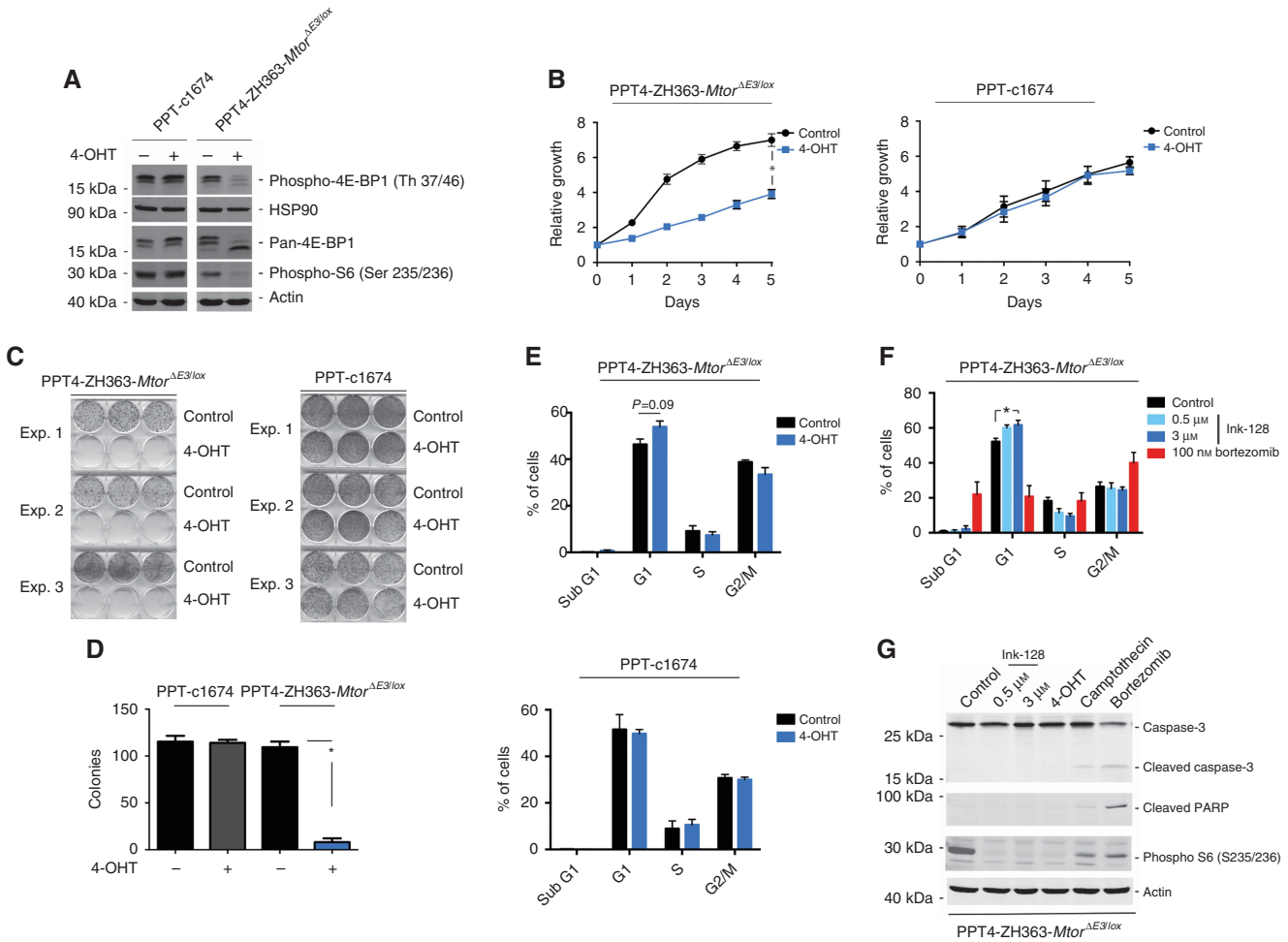

Figure 2. Inactivation of Mtor reduces growth of murine PDAC cells. (**A**) Western blot of phospho- and pan-4E-BP1, and phospho-S6 from vehicle- or 4-OHT- (600 nM) treated cells after 8 days of treatment. Same extracts were blotted to different membranes and loading was controlled by actin or heat-shock protein 90 (HSP90) ($n = 3$). (**B**) Indicated cells were vehicle or 4-OHT (600 nM) treated. After 8 days of treatment, equal number of cells was transferred to 96-well plates and viability was measured over the indicated time points. Shown is the relative growth of the cells and for comparison growth at day 0 was arbitrary set to one. *P-value of an analysis of variance (ANOVA) test <0.05 ($n = 3$). (**C**) Indicated cells were vehicle or 4-OHT (600 nM) treated. After 8 days of treatment, equal number of cells was used to conduct clonogenic assays. Three independent biological replicates were depicted. (**D**) Quantification of (**C**). *P-value of a paired Student's t-test <0.05. (**E**) Indicated cells were vehicle or 4-OHT (600 nM) treated. After 8 days, cells were stained with propidium iodide (PI) and used for cell-cycle fluorescence-activated cell sorting (FACS) analysis. The P-value of a Student's t-test is indicated. (**F**) Indicated cells were treated as indicated for 24 h or were left as vehicle-treated controls. Cells were stained with PI and used for cell-cycle FACS analysis. *P-value of an ANOVA test <0.05 ($n = 3$). (**G**) Indicated cells were treated for 24 h with INK-128, camptothecin (20 µM) or bortezomib (100 nM), or were left as vehicle-treated controls. In addition, cells were treated with 4-OHT (600 nM) over 8 days. Western blot of caspase-3, cleaved poly (ADP-ribose) polymerase (PARP) and phospho-S6. Actin: loading control. Same lysates were blotted to different membranes ($n = 3$).

viability of the cells over time was measured. Compared to vehicle-treated controls, genetic blockade of the MTOR pathway significantly impaired growth (Figure 2B). Growth of the murine PDAC control cell line was not changed upon 4-OHT treatment, thus again excluding tamoxifen and Cre toxicities (Figure 2B). In addition, clonogenic growth was significantly reduced upon deletion of the *Mtor* allele (Figures 2C and D). In FACS assays, an increase of the cells in the G1 phase of the cell cycle upon genetic MTOR inhibition was observed (Figure 2E). No overt increase in the sub-G1 fraction was detected (Figure 2E). Cell-cycle distribution was not altered in control cells (Figure 2E). To corroborate these results, we used the dual mTORC1/TORC2 inhibitor INK-128 (Hsieh *et al*, 2012). This inhibitor has a high potency towards MTOR (inhibition constant 1.4 nM) and is currently tested in clinical studies. INK-128 blocks AKT, S6 and 4E-BP1 phosphorylation (Supplementary Figure 6A). The cellular effect of INK-128 is diminished in *Mtor*-deleted PDAC cells (Supplementary Figure 6B), arguing that INK-128 acts at least in part via MTOR. Consistent with the genetic deletion of *Mtor*, INK-128 treatment increased the fraction of cells in the G1 phase of the cell cycle (Figure 2F). Whereas the proteasome inhibitor bortezomib, used as a positive control for induction of apoptosis, increased the sub-G1 fraction of cells, no distinct increase was observed upon the treatment with INK-128 (Figure 2F). Consistently, while treatment with bortezomib and the chemotherapeutic camptothecin was followed by cleavage of caspase-3 and the caspase substrate PARP, neither INK-128 nor genetic deletion of *Mtor* induced such changes (Figure 2G). Taken together, the genetic as well as the pharmacological data argue that MTOR inhibition acts cytostatic in the investigated model.

MTOR is connected to metabolic programmes of PDAC cells. To find pathways and processes connected to MTOR in PDAC cells, we analysed RNA-Seq data of 4-OHT-treated PPT4-

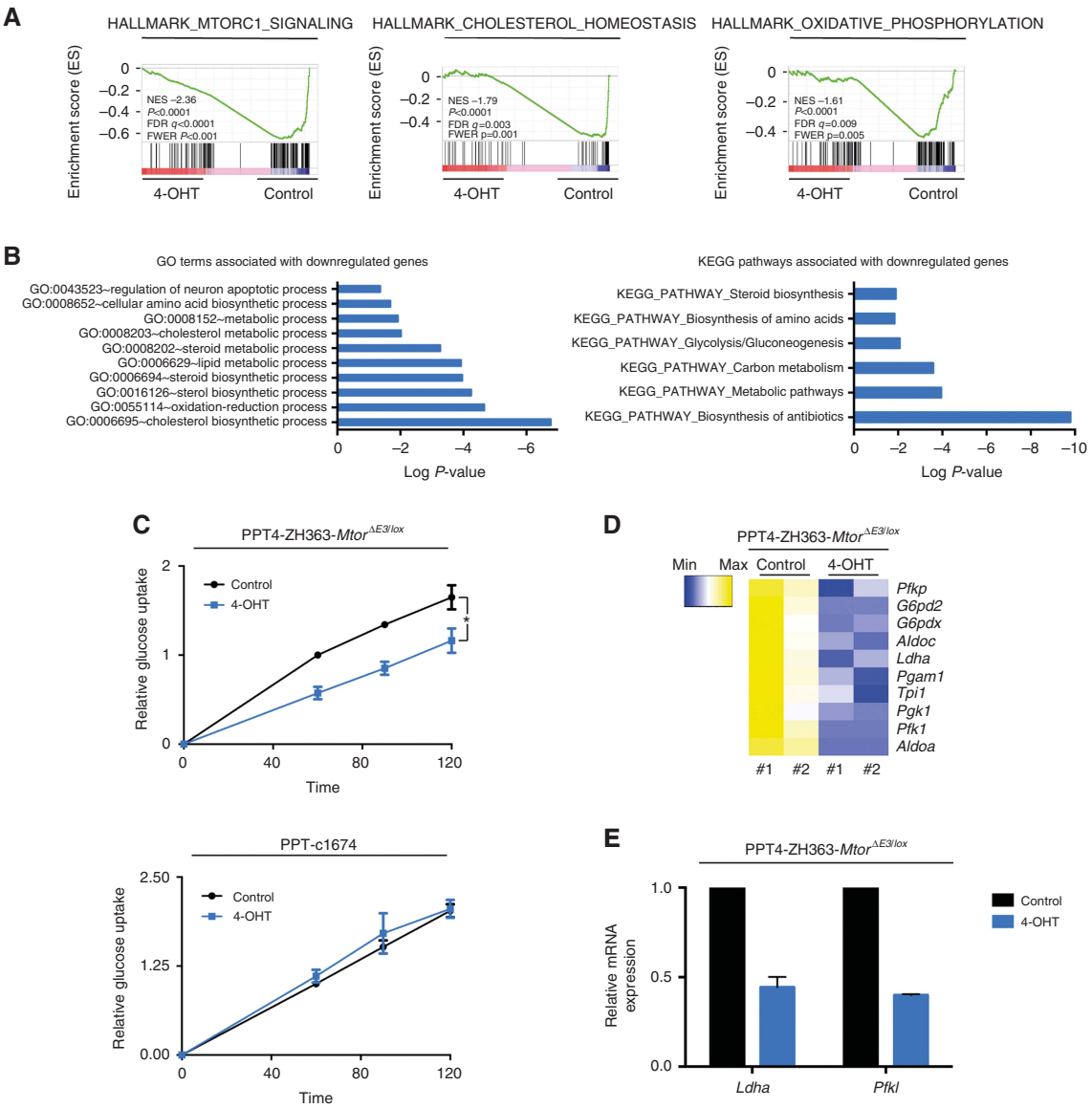

Figure 3. Mtor is connected to metabolic pathways. (**A**) PPT4-ZH363-*Mtor*$^{\Delta E3/lox}$ cells were treated with vehicle or 4-OHT (600 nM) over 8 days. Afterwards, mRNA expression of two biological replicates was profiled using RNA-Seq and analysed by GSEA. The normalised enrichment score (NES), nominal *P*-value, FDR *q*-value and FWER *P*-values are indicated. (**B**) GO-Term and KEGG pathway analysis was conducted with genes downregulated (log 2FC $\leqslant -0.58$) upon the *Mtor* deletion using the RNA-Seq data from (**A**). Terms and pathways with a Benjamini-corrected *P*-value <0.05 were depicted. (**C**) PPT4-ZH363-*Mtor*$^{\Delta E3/lox}$ or control PPT-c1674 cells were treated with vehicle or 4-OHT (600 nM) over 8 days. Afterwards, equal number of cells was analysed for glucose uptake over time using F-18-FDG uptake assay. **P*-value of an analysis of variance (ANOVA) test <0.05 ($n=4$). (**D**) Heat map of glycolytic enzymes from RNA-Seq data described in (**A**). (**E**) PPT4-ZH363-*Mtor*$^{\Delta E3/lox}$ cells were treated with vehicle or 4-OHT (600 nM) over 8 days. Afterwards, mRNA expression of *Ldha* and *Pfkl* mRNA expression was determined by qPCR using *beta-actin* mRNA expression as reference ($n=2$).

ZH363-*Mtor*$^{\Delta E3/lox}$ cells, using GSEA, GO and KEGG pathway analysis. In addition to MTOR signalling, signatures and pathways connected to metabolism were associated with genes downregulated upon *Mtor* deletion (Figures 3A and B, Supplementary Table 1), arguing that MTOR significantly contributes to maintain these pathways. *Kras*^{G12D} signalling drives the glucose uptake of murine PDAC cells to promote ribose biogenesis and proliferation (Ying *et al*, 2012). Consistent with a function as an important downstream effector of KRAS, glucose uptake was significantly decreased in *Mtor*-deleted murine PDAC cells (Figure 3C). Neither 4-OHT nor Cre influences glucose uptake in control cells (Figure 3C). In addition, expression of enzymes involved in glucose metabolism, including *Ldha* and *PfkI*, decreased upon the genetic inactivation of *Mtor* (Figures 3D and E). To test the relevance of the MTOR-connected glycolytic enzymes in human PDAC, we accessed RNA-Seq expression data (Bailey *et al*, 2016). Cluster analysis of expression of the glycolytic enzymes demonstrates a PDAC subgroup (12.5%) with high expression of these enzymes (Supplementary Figure 7A). Consistently, a glycolytic PDAC subtype, detected by metabolic profiling, has been described (Daemen *et al*, 2015). Beyond glycolytic signatures, we observed MTORC1 signatures, hypoxia signatures and epithelial-to-mesenchymal transition signatures in the PDACs with high expression of the glycolytic enzymes (Supplementary Figure 7B). In addition, high *LDHA* mRNA expression marks PDACs with a worse prognosis (Supplementary Figure 7C), in line with recent observations (He *et al*, 2015; Mohammad *et al*, 2016). Such data argue that the MTOR-connected glycolytic enzymes (Figure 3D)

are relevant for human PDAC and support the connection of MTOR signalling to glycolysis in this human PDAC subgroup.

Adaptive rewiring of driver pathways upon *Mtor* deletion. Early adaptive rewiring of signalling pathways upon intervention with targeted therapeutics is an important resistance mechanism (Chandarlapaty, 2012). To find adaptive signalling processes occurring after deletion of *Mtor* we focused on two main driver pathways in PDAC, the ERK and the PI3K signalling pathways. As shown in Figure 4A, increased phosphorylation of AKT, as a surrogate for PI3K pathway activity, as well as an increased phosphorylation of ERK were observed upon *Mtor* deletion.

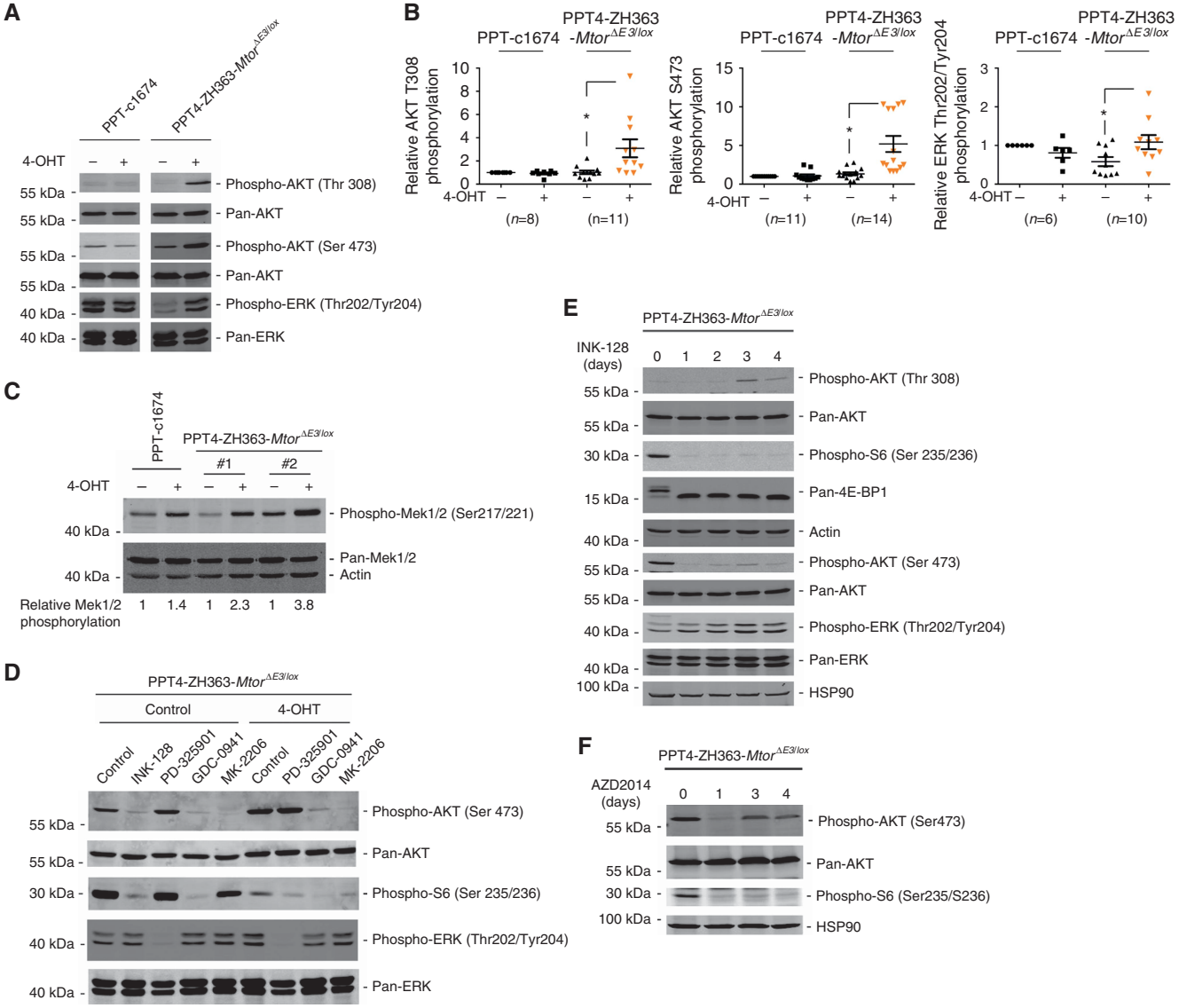

Figure 4. Adaptive rewiring upon *Mtor* deletion in murine PDAC cells. (**A**) PPT4-ZH363-*Mtor*$^{\Delta E3/lox}$ or control PPT-c1674 cells were treated with vehicle or 4-OHT (600 nM) over 8 days. Western blot determines phosphorylation and expression of AKT (Thr308 and Ser473) as well as ERK (Thr202/Tyr204). Same lysates were blotted to different membranes and controlled by pan-AKT or pan-ERK for equal loading. (**B**) PPT4-ZH363-*Mtor*$^{\Delta E3/lox}$ or control PPT-c1674 cells were treated with vehicle or 4-OHT (600 nM) over 8 days. Quantification of independent biological replicates of phosphorylation of AKT at Thr308 and Ser473 as well as ERK at Thr202 and Tyr 204. The ratio of the depicted phospho-protein to the pan-protein in untreated control PPT-c1674 cells was arbitrary set to one. The number of replicates is depicted. **P*-value of a paired Student's *t*-test <0.05. (**C**) Indicated cells were treated as in (**A**). Western blot determines phosphorylation of Mek1/2 at Ser217/221 and expression of Mek1/2. Actin: loading control. Experiment was performed once in PPT-c1674 cells and twice (#1, #2) in PPT4-ZH363-*Mtor*$^{\Delta E3/lox}$ cells. All replicates were blotted to the same membrane. The ratio of phosphorylated to pan-Mek1/2 was determined and arbitrary set to 1 in vehicle-treated cells. The relative Mek1/2 phosphorylation is depicted. (**D**) Indicated cells were treated as described in (**A**). Afterwards, cells were treated for 6 h with INK-128 (2 μM), PD-325901 (2 μM), GDC-0941 (4 μM) or MK-2206 (4 μM). Western blot of phospho- (Ser473) and pan-AKT, phospho-S6 (Ser235/Ser236), phospho- (Thr202/Tyr204) and pan-ERK ($n=2$). (**E**) PPT4-ZH363-*Mtor*$^{\Delta E3/lox}$ cells were treated over time as indicated with INK-128 (0.5 μM). Western blot of phospho- (Thr308 and Ser473), pan-AKT, phospho-S6 (Ser235/Ser236), phospho- (Thr202/Tyr204) and pan-ERK. Heat-shock protein 90 (HSP90) and actin: loading control. Same lysates were blotted to different membranes ($n=2$). (**F**) PPT4-ZH363-*Mtor*$^{\Delta E3/lox}$ cells were treated over time as indicated with AZD2014 (0.5 μM). Western blot of phospho-Ser473 and pan-AKT, phospho-S6 (Ser235/Ser236), HSP90: loading control. Same lysates were blotted to different membranes ($n=3$). For (**E**) and (**F**) medium with fresh inhibitors or vehicle was replaced each day.

Quantification of independent biological replicates yields a significantly increased phosphorylation of AKT at Thr308 and Ser473 as well as ERK upon the genetic deletion of *Mtor* (Figure 4B). To gain further insight into the level at which signalling rewiring occurs, we firstly determined phosphorylation of MEK. Applying an antibody which detects Ser217/221 phosphorylated MEK1/2, we observed increased phosphorylation of MEK1/2 upon deletion of *Mtor* (Figure 4C). Second, we used the PI3K (GDC-0941), AKT (MK-2206) or MEK (PD-325901) inhibitors, in addition to INK-128 (Hsieh *et al*, 2012). No influence of the MEK inhibitor towards AKT phosphorylation was detected irrespective of the presence of MTOR (Figure 4D). This inhibitor mainly blocks canonical ERK signalling. The PI3K and the AKT inhibitor block AKT and S6 phosphorylation to different extents in the MTOR-proficient and -deficient setting (Figure 4D). No effect of either inhibitor toward ERK phosphorylation was evident (Figure 4D). In summary, these data may point to a process upstream of MEK and AKT engaged upon the deletion of *Mtor*.

To recapitulate such effects observed in the genetic model at the pharmacological level, INK-128 was used over a time period of 4 days. Blockade of MTOR was monitored by the presence of hypophosphorylated 4E-BP1 and decreased phosphorylation of S6 (Figure 4E). We detected increased phosphorylation of AKT Thr308 after 3 days of INK-128 treatment (Figure 4E). AKT Ser473 phosphorylation was decreased after 24 h of INK-128 treatment, while, in comparison with 24 h, a slightly increased phosphorylation was observed at day 3 (Figure 4E). Compared to the reactivation of the PI3K-AKT pathway, phosphorylation of ERK was detected earlier in the time course of INK-128 treatment (Figure 4E). Recent investigations demonstrated that AKT Ser473 phosphorylation is significantly blocked in murine PDAC *in vivo* upon dual MTOR inhibition (Driscoll *et al*, 2016). Therefore, to further consolidate our observations we used another dual MTOR inhibitor, AZD2014 (Pike *et al*, 2013). Again, AKT Ser473 phosphorylation was significantly decreased 24 h after treatment of cells with AZD2014 (Figure 4F). However, an increase of AKT Ser473 phosphorylation was observed at days 3 and 4 upon continuous treatment with AZD2014 (Figure 4F). Blockade of MTOR was verified by investigating phosphorylation of S6, which was impaired during the treatment period (Figure 4F), demonstrating potent MTOR inhibition in the experimental setting. Important recent work has demonstrated that the noncanonical IκB-related kinase IKBKE phosphorylates Ser473 of AKT upon dual MTOR inhibition (Rajurkar *et al*, 2017). To test the contribution of IKBKE for AKT Ser473 phosphorylation upon genetic *Mtor* deletion, we used the IKBKE inhibitor MRT67307 (Clark *et al*, 2011, 2012). Again, genetic deletion of *Mtor* increased phosphorylation of Ser473 of AKT (Supplementary Figure 8). This effect was diminished upon the treatment of *Mtor*-deleted cells with MRT67307 (Supplementary Figure 8). Therefore, our data support the recent report (Rajurkar *et al*, 2017) and might point to a role of IKBKE in adaption upon dual MTOR inhibition.

In sum, we conclude that rewiring of signalling occurs also after the pharmacological blockade of the MTOR kinase and is therefore an important resistance mechanism. The discrepant extent of reactivation of the pathways in the genetic and pharmacological models might be explained by different time points analysed, off-target effects of the inhibitor or threshold effects upon partial inhibition of the kinase.

Deciphering dual MTOR inhibitor-based combination therapies. Activation of the ERK and the PI3K pathway upon inhibition of MTOR prompted us to test the dual MTOR inhibitor INK-128 together with PI3K (GDC-0941), AKT (MK-2206) or MEK (PD-325901) inhibitors in human and murine PDAC models, respectively. Efficacy of INK-128 was increased to different extents in the investigated models by combined PI3K, AKT or MEK inhibition. Figure 5A demonstrates the dose response of INK-128 in a human and murine PDAC cell line in the presence and absence of MK-2206, GDC-0941 or PD-325901. A favourable response of these combinations was also detected in clonogenic assays (Supplementary Figure 9). In Supplementary Table 2, the influence of the PI3K, AKT or MEK inhibitor to the INK-128 GI_{50} of 14 human and murine 2D PDAC cell lines is represented.

To further extend the notion that the combined inhibition of MTOR and the PI3K or canonical KRAS-MEK-ERK pathway is a therapeutic option for PDAC, we used primary human PDAC 3D culture models. Such technology provides the unique opportunity to investigate therapeutic approaches in a human model system, which recapitulates relevant aspects of the disease (Baker *et al*, 2016). Again, human primary PDAC 3D cultures were more sensitive to INK-128 in case of AKT, PI3K or MEK coinhibition (Figure 5B and Supplementary Table 2). To compare these combination therapies across species and models, the SC was calculated (Figure 5C). The SC was heterogeneously distributed for the individual combination as well as the individual model (Figure 5C). Heterogeneity of the response of the investigated combination is further underscored by the observation that the SCs for the MTOR/AKT inhibitor combination and the MTOR/PI3K inhibitor combination significantly correlate, whereas the scores of both combinations to the MTOR/MEK inhibitor combination do not (Supplementary Figure 10). Analysing all used PDAC models, the mean SC was highest for the combination of the MTOR inhibitor with the MEKi inhibitor (mean score 1.34), followed by the combination of the MTOR inhibitor with the PI3Ki (mean score 1.09) (Figure 5D). The SC was lowest for the combination of the MTOR inhibitor with the AKTi (mean score 0.71) (Figure 5D). Taken together, blocking adaptive rewiring of oncogenic signalling upon MTOR inhibition is relevant in some of the investigated PDAC models.

DISCUSSION

Although preclinical data suggest activity of mTORC1 inhibitors in a PDAC subgroup with hyperactivation of the PI3K-mTOR pathway (Garrido-Laguna *et al*, 2010; Morran *et al*, 2014), clinical data in non-stratified patients failed to demonstrate a benefit (Garrido-Laguna *et al*, 2010; Javle *et al*, 2010). There is clear evidence that mTORC1 directs complex negative feedback loops to restrain upstream signalling. Inhibitors of mTORC1 can drive activation of PI3K-, AKT- or ERK-directed pathways (Rozengurt *et al*, 2014) and the feedback phosphorylation of Ser473 of AKT by mTORC2 in response to rapalogues is a prominent example (Rozengurt *et al*, 2014). Such feedback signalling limits the efficacy of targeted therapies (Chandarlapaty, 2012).

To completely block MTOR signalling and to increase clinical efficacy, dual ATP-competitive inhibitors were developed. The dual mTORC1/TORC2 inhibitor AZD2014 prolonged survival in an aggressive PDAC mouse model, which relies on the simultaneous expression of the $Kras^{G12D}$ oncogene and the mutated tumour suppressor $p53^{R172H}$ (Driscoll *et al*, 2016). Such data argue that dual mTORC1/TORC2 inhibitor-based therapies are therapeutic options in PDAC. To further support such a note and to mimic specific dual mTORC1/TORC2 inhibitors, we developed a novel model, allowing the genetic inactivation of MTOR in PDAC cells. Upon MTOR inactivation or inhibition, impaired growth with accumulation of cells in the G1 phase of the cell cycle was detected. Mechanistically, inhibition of MTOR at the genetic level affects multiple metabolic pathways. We demonstrate impaired glucose uptake upon MTOR deletion and a reduced expression of glycolytic enzymes, which are relevant in a subgroup of the human

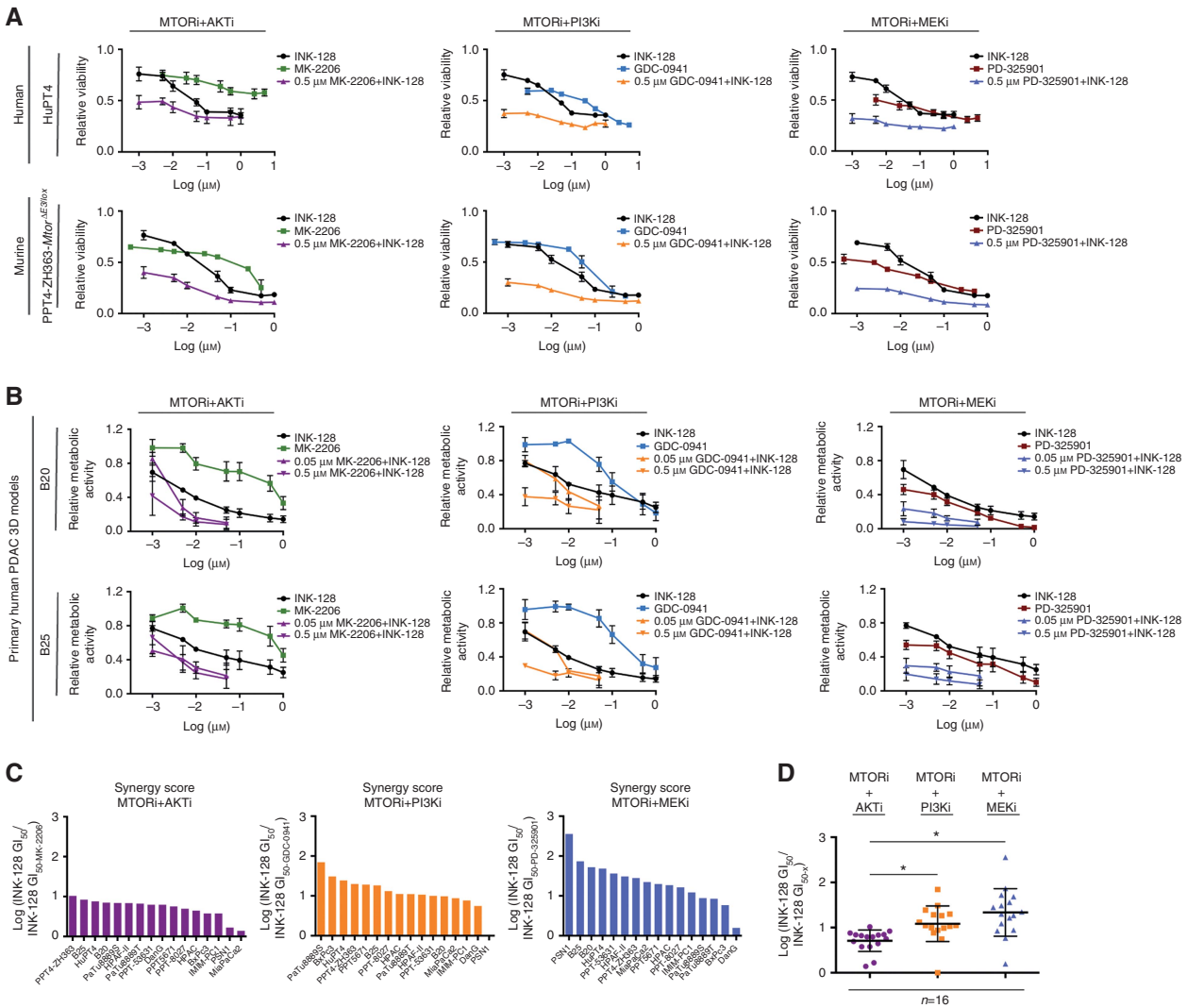

Figure 5. MTOR-based combination therapies. (**A**) The indicated human and murine cell lines were treated with INK-128, MK-2206, GDC-0941 or PD-325901, or in combinations thereof as indicated. After 72 h, viability was measured in MTT assays. Viability of vehicle-treated control cells was arbitrarily set to 1. (**B**) Primary human PDAC 3D cultures B20 and B25 were treated with INK-128, MK-2206, GDC-0941 or PD-325901, or in combinations thereof as indicated. After 5 days, ATP levels were measured using a luminometric viability assay. Metabolic activity of untreated cells was arbitrarily set to 1. (**C**) Synergy score for the combination of the MTOR inhibitor (INK-128) with the AKT (MK-2206), PI3K (GDC-0941) and MEK (PD-325901) inhibitor in 10 human PDAC cell lines, 4 murine PDAC cell lines and 2 primary human PDAC 3D cultures. (**D**) Comparison of the synergy scores of (**C**). **P*-value of analysis of variance (ANOVA) test <0.05.

disease. Since it is described that glucose in murine PDAC cells fluxes into the pentose phosphate pathway needed for ribose biogenesis (Ying *et al*, 2012), reduced availability of nucleotides may contribute to the impaired growth of *Mtor*-deleted PDAC cells with accumulation of cells in the G1 phase of the cell cycle. Although we did not observe induction of apoptosis upon MTOR inactivation or inhibition, other cell fate decisions may contribute to the observed effects.

Early after the deletion or inhibition of the MTOR kinase in murine PDAC cells, we detected adaptive activation of the canonical ERK and PI3K-AKT pathways. Increased phosphorylation of Thr308 as well as Ser473 of AKT was detected. Phosphorylation of Ser473 upon MTOR deletion is consistent with a recent publication, demonstrating phosphorylation of Ser473 of AKT upon treatment of PDAC cells with the dual mTORC1/TORC2 inhibitor Torin-1 (Rajurkar *et al*, 2017). Here, the noncanonical IκB-related kinase IKBKE was characterised as an important alternative AKT kinase in PDAC (Rajurkar *et al*, 2017). We observed that increased phosphorylation of Ser473 of AKT upon *Mtor* deletion was partially blocked by MRT67307, an inhibitor which targets IKBKE (Clark *et al*, 2011, 2012). Although we cannot exclude 'off-target' effects of MRT67307 contributing to the observed regulation, our data are supportive for the above-mentioned study. Whereas Rajurkar *et al* (2017) and our study provide evidence that AKT Ser473 re-phosphorylation occurs upon dual MTOR inhibition in PDAC cells, AKT Ser473 remains blocked in PDAC *in vivo* models (Driscoll *et al*, 2016). Such discrepant findings may be explained by different detection thresholds in western blotting *vs* immunohistochemistry or diverse effective dosages in the *in vitro* and *in vivo* settings. Furthermore, future experiments should address whether AKT involving rewiring mechanisms are generally observed in PDAC or restricted to subtypes and linked to response heterogeneity.

Activation of potent tumour-promoting pathways in response to dual MTOR inhibition in PDAC models (our work and Rajurkar *et al* (2017) and Wei *et al* (2015)), the progression of tumours in the KPC mouse models despite dual MTOR inhibition (Driscoll *et al*, 2016) and the lack of therapeutic effects of genetic or

pharmacological MTOR inhibition in certain human *in vivo* models (Wei *et al*, 2015; Rajurkar *et al*, 2017) argues to establish dual MTOR inhibitor-based combination therapies. To address the reactivation of both driver pathways in response to MTOR inhibition, we tested INK-128 with the MEKi PD-325901, the PI3Ki GDC-0941 or the AKTi MK-2206. Here, SC was highest for the combination of INK-128 and PD-325901 and some PDAC models show an up to a 350-fold increased sensitivity towards the dual MTOR inhibitor if MEK is blocked. The value of a combined inhibition of MEK and mTORC1/TORC2 was already analysed in other preclinical tumour models, including respective models of lung cancer (Holt *et al*, 2012), rhabdomyosarcoma (Renshaw *et al*, 2013) or uveal melanoma (Ho *et al*, 2012). In colorectal cancer, MEK inhibition combined with mTORC1/TORC2 inhibition may show efficacy in context of a p53 wild-type status (Garcia-Garcia *et al*, 2015). The molecular and genetic determinates predicting synergy in PDAC await further investigations.

In addition, we observed a considerable response in some of the investigated PDAC models towards the combination of mTORC1/TORC2 inhibition with PI3K inhibition. Consistently, the combination of a dual mTORC1/TORC2 inhibitor (AZD2014) with a PI3K inhibitor (AZD8186; proposed to be a PI3Kβ inhibitor) was active in the above-mentioned PDAC *in vivo* model (Driscoll *et al*, 2016). The observation that the combination of mTORC1/TORC2 inhibition with AKT inhibition is least effective in the investigated PDAC models might be explained by more than the AKT pathway branching out of the PI3K-PDK1 node.

Increased MEK-ERK as well as AKT Thr308 phosphorylation upon a complete block of MTOR may be activated by a signal upstream of both pathways. Consistently, AKT phosphorylation in MTOR-deleted cells was sensitive to PI3Ki and ERK phosphorylation to MEKi but not *vice versa*. A possibility is the activation of upstream receptor tyrosine kinases (RTKs) accounting for activation of both driver pathways upon complete MTOR blockade. Indeed, in endothelial cells, mTORC1/TORC2 inhibitors were found to induce a profound reprograming and activation of RTKs, including the epidermal growth factor receptor (EGFR), the vascular endothelial growth factor receptor 2, the insulin-like growth factor 1 receptor or the insulin receptor (Zhuang *et al*, 2013). Congruently, RTK-dependent adaptive responses occurring upon the blockade of relevant driver pathways were described in numerous cancer models involving different molecular mechanisms (Prahallad *et al*, 2012; Bai *et al*, 2014; Yoshida *et al*, 2014; Obenauf *et al*, 2015; Kim *et al*, 2016). Feedback activation of the EGFR upon dual MTOR inhibition was also described in human PDAC cells (Wei *et al*, 2015). Considering such a scenario, future work might consider triple therapies (e.g., mTORC1/TORC2, MEKi and PI3Ki) or broad-acting RTK inhibitor combinations with dual mTORC1/TORC2 inhibitors to interfere with both branches of adaptive signalling. However, toxicity might limit clinical use of such combinations and alternative dosing and scheduling regimens are needed. In addition to RTK-dependent adaption, it is important to consider that canonical RAS-ERK signalling can be tuned at multiple levels. Since MTOR changes cellular metabolism of PDAC cells, connections of metabolism to signalling outputs might contribute. As an example, in melanoma cells, the ketone body acetoacetate was demonstrated to contribute to canonical RAS-ERK activity by promoting the interaction of $BRAF^{V600E}$ with MEK1 (Kang *et al*, 2015), underscoring the tight connection of signalling outputs to metabolic states.

The systematic analysis of the combined inhibition of MTOR with MEK, PI3K or AKT points to a considerable heterogeneity of the cellular response towards the used combination therapies. In some of the investigated models the impact of the tested combination therapies is minor. These data implement that robust markers have to be developed to stratify for responsive PDAC subgroups and that clinical testing without prior selection will fail. Such considerations are underscored by recent preclinical and clinical observations, which aimed to target the PI3K and MEK-ERK pathways in PDAC. The combination of a MEKi and a PI3Ki induced a partial response (>30% reduction in tumour volume) in only ~13% of animals in a PDAC mouse model generated by the activation $Kras^{G12D}$ and simultaneous inactivation of *Cdkn2a* (Junttila *et al*, 2015) and in 50% of animals in a PDAC mouse model generated by the activation $Kras^{G12D}$ and simultaneous inactivation of *p53* (Alagesan *et al*, 2015). In the clinic, a recent trial in patients with metastatic PDAC after failure of gemcitabine-based first-line therapy demonstrated a partial response towards a MEKi (AZD-6244; selumetinib) and AKTi (MK-2206) combination therapy in only 1.7% (Chung *et al*, 2016).

Although it is currently unclear whether the downstream blockade (e.g., mTORC1/TORC2 inhibitors) of the PI3K-AKT-MTOR pathway is superior to upstream interventions (e.g. PI3Ki or AKTi), our data combined with recent work in PDAC mouse models (Driscoll *et al*, 2016) argue for an option to develop mTORC1/TORC2 inhibitor-based combination therapies for a PDAC subgroup. Therefore, further work needs to include (I) predictive biomarkers for mTORC1/TORC2 inhibitor-based therapies, (II) a detailed molecular understanding of adaptive rewiring of oncogenic pathways upon mTORC1/TORC2 inhibition and (III) unbiased MTOR-centred synthetic lethality screens to increase the chance to successfully establish dual MTOR inhibitor-based therapies.

ACKNOWLEDGEMENTS

We thank Dr P Soriano and Dr L Luo for providing mouse lines. We thank Dr A Bradley for support and help during the transfer of mouse lines. We thank the Z1 Project of the SFB824 for providing radiotracers. The depicted results of Supplementary Figure 7C are in whole based on data that were generated by the TCGA Research Network: http://cancergenome.nih.gov/. This work was supported by the Deutsche Forschungsgemeinschaft (DFG) (SFB824/C9 to GS and DS; SCHN 959/3-1 to GS), Deutsche Krebshilfe (111273 (Max-Eder Program) to MR), Wilhelm-Sander Foundation (2016.004.1 to GS), DKTK Joint Funding (to RR, DS, WW and GS), Else-Kröner-Fresenius-Stiftung (to 2016_A43 to MW).

CONFLICT OF INTEREST

The authors declare no conflict of interest.

REFERENCES

Afgan E, Baker D, van den Beek M, Blankenberg D, Bouvier D, Cech M, Chilton J, Clements D, Coraor N, Eberhard C, Gruning B, Guerler A, Hillman-Jackson J, Von Kuster G, Rasche E, Soranzo N, Turaga N, Taylor J, Nekrutenko A, Goecks J (2016) The Galaxy platform for accessible, reproducible and collaborative biomedical analyses: 2016 update. *Nucleic Acids Res* **44**(W1): W3–W10.

Alagesan B, Contino G, Guimaraes AR, Corcoran RB, Deshpande V, Wojtkiewicz GR, Hezel AF, Wong KK, Loda M, Weissleder R, Benes C, Engelman JA, Bardeesy N (2015) Combined MEK and PI3K inhibition in a mouse model of pancreatic cancer. *Clin Cancer Res* **21**(2): 396–404.

Babicki S, Arndt D, Marcu A, Liang Y, Grant JR, Maciejewski A, Wishart DS (2016) Heatmapper: web-enabled heat mapping for all. *Nucleic Acids Res* **44**(W1): W147–W153.

Baer R, Cintas C, Dufresne M, Cassant-Sourdy S, Schonhuber N, Planque L, Lulka H, Couderc B, Bousquet C, Garmy-Susini B, Vanhaesebroeck B, Pyronnet S, Saur D, Guillermet-Guibert J (2014) Pancreatic cell plasticity and cancer initiation induced by oncogenic Kras is completely dependent on wild-type PI 3-kinase p110alpha. *Genes Dev* **28**(23): 2621–2635.

Bai Y, Kim JY, Watters JM, Fang B, Kinose F, Song L, Koomen JM, Teer JK, Fisher K, Chen YA, Rix U, Haura EB (2014) Adaptive responses to dasatinib-treated lung squamous cell cancer cells harboring DDR2 mutations. *Cancer Res* **74**(24): 7217–7228.

Bailey P, Chang DK, Nones K, Johns AL, Patch AM, Gingras MC, Miller DK, Christ AN, Bruxner TJ, Quinn MC, Nourse C, Murtaugh LC, Harliwong I, Idrisoglu S, Manning S, Nourbakhsh E, Wani S, Fink L, Holmes O, Chin V, Anderson MJ, Kazakoff S, Leonard C, Newell F, Waddell N, Wood S, Xu Q, Wilson PJ, Cloonan N, Kassahn KS, Taylor D, Quek K, Robertson A, Pantano L, Mincarelli L, Sanchez LN, Evers L, Wu J, Pinese M, Cowley MJ, Jones MD, Colvin EK, Nagrial AM, Humphrey ES, Chantrill LA, Mawson A, Humphris J, Chou A, Pajic M, Scarlett CJ, Pinho AV, Giry-Laterriere M, Rooman I, Samra JS, Kench JG, Lovell JA, Merrett ND, Toon CW, Epari K, Nguyen NQ, Barbour A, Zeps N, Moran-Jones K, Jamieson NB, Graham JS, Duthie F, Oien K, Hair J, Grutzmann R, Maitra A, Iacobuzio-Donahue CA, Wolfgang CL, Morgan RA, Lawlor RT, Corbo V, Bassi C, Rusev B, Capelli P, Salvia R, Tortora G, Mukhopadhyay D, Petersen GM, Australian Pancreatic Cancer Genome IMunzy DM, Fisher WE, Karim SA, Eshleman JR, Hruban RH, Pilarsky C, Morton JP, Sansom OJ, Scarpa A, Musgrove EA, Bailey UM, Hofmann O, Sutherland RL, Wheeler DA, Gill AJ, Gibbs RA, Pearson JV, Waddell N, Biankin AV, Grimmond SM (2016) Genomic analyses identify molecular subtypes of pancreatic cancer. *Nature* **531**(7592): 47–52.

Baker LA, Tiriac H, Clevers H, Tuveson DA (2016) Modeling pancreatic cancer with organoids. *Trends Cancer* **2**(4): 176–190.

Beirowski B, Babetto E, Golden JP, Chen YJ, Yang K, Gross RW, Patti GJ, Milbrandt J (2014) Metabolic regulator LKB1 is crucial for Schwann cell-mediated axon maintenance. *Nat Neurosci* **17**(10): 1351–1361.

Boj SF, Hwang CI, Baker LA, Chio, Engle DD, Corbo V, Jager M, Ponz-Sarvise M, Tiriac H, Spector MS, Gracanin A, Oni T, Yu KH, van Boxtel R, Huch M, Rivera KD, Wilson JP, Feigin ME, Ohlund D, Handly-Santana A, Ardito-Abraham CM, Ludwig M, Elyada E, Alagesan B, Biffi G, Yordanov GN, Delcuze B, Creighton B, Wright K, Park Y, Morsink FH, Molenaar IQ, Borel Rinkes IH, Cuppen E, Hao Y, Jin Y, Nijman IJ, Iacobuzio-Donahue C, Leach SD, Pappin DJ, Hammell M, Klimstra DS, Basturk O, Hruban RH, Offerhaus GJ, Vries RG, Clevers H, Tuveson DA (2015) Organoid models of human and mouse ductal pancreatic cancer. *Cell* **160**(1-2): 324–338.

Cao P, Maira SM, Garcia-Echeverria C, Hedley DW (2009) Activity of a novel, dual PI3-kinase/mTor inhibitor NVP-BEZ235 against primary human pancreatic cancers grown as orthotopic xenografts. *Br J Cancer* **100**(8): 1267–1276.

Chandarlapaty S (2012) Negative feedback and adaptive resistance to the targeted therapy of cancer. *Cancer Discov* **2**(4): 311–319.

Chung V, McDonough S, Philip PA, Cardin D, Wang-Gillam A, Hui L, Tejani MA, Seery TE, Dy IA, Al Baghdadi T, Hendifar AE, Doyle LA, Lowy AM, Guthrie KA, Blanke CD, Hochster HS (2016) Effect of selumetinib and MK-2206 vs oxaliplatin and fluorouracil in patients with metastatic pancreatic cancer after prior therapy: SWOG S1115 Study Randomized Clinical Trial. *JAMA Oncol* **3**(4): 516–522.

Clark K, MacKenzie KF, Petkevicius K, Kristariyanto Y, Zhang J, Choi HG, Peggie M, Plater L, Pedrioli PG, McIver E, Gray NS, Arthur JS, Cohen P (2012) Phosphorylation of CRTC3 by the salt-inducible kinases controls the interconversion of classically activated and regulatory macrophages. *Proc Natl Acad Sci USA* **109**(42): 16986–16991.

Clark K, Peggie M, Plater L, Sorcek RJ, Young ER, Madwed JB, Hough J, McIver EG, Cohen P (2011) Novel cross-talk within the IKK family controls innate immunity. *Biochem J* **434**(1): 93–104.

Daemen A, Peterson D, Sahu N, McCord R, Du X, Liu B, Kowanetz K, Hong R, Moffat J, Gao M, Boudreau A, Mroue R, Corson L, O'Brien T, Qing J, Sampath D, Merchant M, Yauch R, Manning G, Settleman J, Hatzivassiliou G, Evangelista M (2015) Metabolite profiling stratifies pancreatic ductal adenocarcinomas into subtypes with distinct sensitivities to metabolic inhibitors. *Proc Natl Acad Sci USA* **112**(32): E4410–E4417.

Diersch S, Wenzel P, Szameitat M, Eser P, Paul MC, Seidler B, Eser S, Messer M, Reichert M, Pagel P, Esposito I, Schmid RM, Saur D, Schneider G (2013) Efemp1 and p27(Kip1) modulate responsiveness of pancreatic cancer cells towards a dual PI3K/mTOR inhibitor in preclinical models. *Oncotarget* **4**(2): 277–288.

Diersch S, Wirth M, Schneeweis C, Jors S, Geisler F, Siveke JT, Rad R, Schmid RM, Saur D, Rustgi AK, Reichert M, Schneider G (2015) KrasG12D induces EGFR-MYC cross signaling in murine primary pancreatic ductal epithelial cells. *Oncogene* **35**(29): 3880–3886.

Driscoll DR, Karim SA, Sano M, Gay DM, Jacob W, Yu J, Mizukami Y, Gopinathan A, Jodrell DI, Evans TR, Bardeesy N, Hall MN, Quattrochi BJ, Klimstra DS, Barry ST, Sansom OJ, Lewis BC, Morton JP (2016) mTORC2 signaling drives the development and progression of pancreatic cancer. *Cancer Res* **76**(23): 6911–6923.

Eser S, Reiff N, Messer M, Seidler B, Gottschalk K, Dobler M, Hieber M, Arbeiter A, Klein S, Kong B, Michalski CW, Schlitter AM, Esposito I, Kind AJ, Rad L, Schnieke AE, Baccarini M, Alessi DR, Rad R, Schmid RM, Schneider G, Saur D (2013) Selective requirement of PI3K/PDK1 signaling for Kras oncogene-driven pancreatic cell plasticity and cancer. *Cancer Cell* **23**(3): 406–420.

Garcia-Garcia C, Rivas MA, Ibrahim YH, Calvo MT, Gris-Oliver A, Rodriguez O, Grueso J, Anton P, Guzman M, Aura C, Nuciforo P, Jessen K, Argiles G, Dienstmann R, Bertotti A, Trusolino L, Matito J, Vivancos A, Chicote I, Palmer HG, Tabernero J, Scaltriti M, Baselga J, Serra V (2015) MEK plus PI3K/mTORC1/2 therapeutic efficacy is impacted by TP53 mutation in preclinical models of colorectal cancer. *Clin Cancer Res* **21**(24): 5499–5510.

Garrido-Laguna I, Tan AC, Uson M, Angenendt M, Ma WW, Villaroel MC, Zhao M, Rajeshkumar NV, Jimeno A, Donehower R, Iacobuzio-Donahue C, Barrett M, Rudek MA, Rubio-Viqueira B, Laheru D, Hidalgo M (2010) Integrated preclinical and clinical development of mTOR inhibitors in pancreatic cancer. *Br J Cancer* **103**(5): 649–655.

Goecks J, Eberhard C, Too T, Galaxy T, Nekrutenko A, Taylor J (2013) Web-based visual analysis for high-throughput genomics. *BMC Genomics* **14**: 397.

He TL, Zhang YJ, Jiang H, Li XH, Zhu H, Zheng KL (2015) The c-Myc-LDHA axis positively regulates aerobic glycolysis and promotes tumor progression in pancreatic cancer. *Med Oncol* **32**(7): 187.

Ho AL, Musi E, Ambrosini G, Nair JS, Deraje Vasudeva S, de Stanchina E, Schwartz GK (2012) Impact of combined mTOR and MEK inhibition in uveal melanoma is driven by tumor genotype. *PLoS One* **7**(7): e40439.

Holt SV, Logie A, Davies BR, Alferez D, Runswick S, Fenton S, Chresta CM, Gu Y, Zhang J, Wu YL, Wilkinson RW, Guichard SM, Smith PD (2012) Enhanced apoptosis and tumor growth suppression elicited by combination of MEK (selumetinib) and mTOR kinase inhibitors (AZD8055). *Cancer Res* **72**(7): 1804–1813.

Hsieh AC, Liu Y, Edlind MP, Ingolia NT, Janes MR, Sher A, Shi EY, Stumpf CR, Christensen C, Bonham MJ, Wang S, Ren P, Martin M, Jessen K, Feldman ME, Weissman JS, Shokat KM, Rommel C, Ruggero D (2012) The translational landscape of mTOR signalling steers cancer initiation and metastasis. *Nature* **485**(7396): 55–61.

Huang, da W, Sherman BT, Lempicki RA (2009) Systematic and integrative analysis of large gene lists using DAVID bioinformatics resources. *Nat Protoc* **4**(1): 44–57.

Javle MM, Shroff RT, Xiong H, Varadhachary GA, Fogelman D, Reddy SA, Davis D, Zhang Y, Wolff RA, Abbruzzese JL (2010) Inhibition of the mammalian target of rapamycin (mTOR) in advanced pancreatic cancer: results of two phase II studies. *BMC Cancer* **10**: 368.

Junttila MR, Devasthali V, Cheng JH, Castillo J, Metcalfe C, Clermont AC, Otter DD, Chan E, Bou-Reslan H, Cao T, Forrest W, Nannini MA, French D, Carano R, Merchant M, Hoeflich KP, Singh M (2015) Modeling targeted inhibition of MEK and PI3 kinase in human pancreatic cancer. *Mol Cancer Ther* **14**(1): 40–47.

Kang HB, Fan J, Lin R, Elf S, Ji Q, Zhao L, Jin L, Seo JH, Shan C, Arbiser JL, Cohen C, Brat D, Miziorko HM, Kim E, Abdel-Wahab O, Merghoub T, Frohling S, Scholl C, Tamayo P, Barbie DA, Zhou L, Pollack BP, Fisher K, Kudchadkar RR, Lawson DH, Sica G, Rossi M, Lonial S, Khoury HJ, Khuri FR, Lee BH, Boggon TJ, He C, Kang S, Chen J (2015) Metabolic rewiring by oncogenic BRAF V600E links ketogenesis pathway to BRAF-MEK1 signaling. *Mol Cell* **59**(3): 345–358.

Kennedy AL, Morton JP, Manoharan I, Nelson DM, Jamieson NB, Pawlikowski JS, McBryan T, Doyle B, McKay C, Oien KA, Enders GH, Zhang R, Sansom OJ, Adams PD (2011) Activation of the PIK3CA/AKT pathway suppresses senescence induced by an activated RAS oncogene to promote tumorigenesis. *Mol Cell* **42**(1): 36–49.

Kim JY, Welsh EA, Fang B, Bai Y, Kinose F, Eschrich SA, Koomen JM, Haura EB (2016) Phosphoproteomics reveals MAPK inhibitors enhance MET- and EGFR-driven AKT signaling in KRAS-mutant lung cancer. *Mol Cancer Res* **14**(10): 1019–1029.

Kong B, Wu W, Cheng T, Schlitter AM, Qian C, Bruns P, Jian Z, Jager C, Regel I, Raulefs S, Behler N, Irmler M, Beckers J, Friess H, Erkan M, Siveke JT, Tannapfel A, Hahn SA, Theis FJ, Esposito I, Kleeff J, Michalski CW (2016) A subset of metastatic pancreatic ductal adenocarcinomas depends quantitatively on oncogenic Kras/Mek/Erk-induced hyperactive mTOR signalling. *Gut* **65**(4): 647–657.

Metsalu T, Vilo J (2015) ClustVis: a web tool for visualizing clustering of multivariate data using principal component analysis and heatmap. *Nucleic Acids Res* **43**(W1): W566–W570.

Mohammad GH, Olde Damink SW, Malago M, Dhar DK, Pereira SP (2016) Pyruvate kinase M2 and lactate dehydrogenase A are overexpressed in pancreatic cancer and correlate with poor outcome. *PLoS One* **11**(3): e0151635.

Morran DC, Wu J, Jamieson NB, Mrowinska A, Kalna G, Karim SA, Au AY, Scarlett CJ, Chang DK, Pajak MZ. Australian Pancreatic Cancer Genome IOien KA, McKay CJ, Carter CR, Gillen G, Champion S, Pimlott SL, Anderson KI, Evans TR, Grimmond SM, Biankin AV, Sansom OJ, Morton JP (2014) Targeting mTOR dependency in pancreatic cancer. *Gut* **63**(9): 1481–1489.

Muzumdar MD, Tasic B, Miyamichi K, Li L, Luo L (2007) A global double-fluorescent Cre reporter mouse. *Genesis* **45**(9): 593–605.

Obenauf AC, Zou Y, Ji AL, Vanharanta S, Shu W, Shi H, Kong X, Bosenberg MC, Wiesner T, Rosen N, Lo RS, Massague J (2015) Therapy-induced tumour secretomes promote resistance and tumour progression. *Nature* **520**(7547): 368–372.

Ossewaarde JM, de Vries A, Bestebroer T, Angulo AF (1996) Application of a Mycoplasma group-specific PCR for monitoring decontamination of Mycoplasma-infected *Chlamydia* sp. strains. *Appl Environ Microbiol* **62**(2): 328–331.

Payne SN, Maher ME, Tran NH, Van De Hey DR, Foley TM, Yueh AE, Leystra AA, Pasch CA, Jeffrey JJ, Clipson L, Matkowskyj KA, Deming DA (2015) PIK3CA mutations can initiate pancreatic tumorigenesis and are targetable with PI3K inhibitors. *Oncogenesis* **4**: e169.

Pike KG, Malagu K, Hummersone MG, Menear KA, Duggan HM, Gomez S, Martin NM, Ruston L, Pass SL, Pass M (2013) Optimization of potent and selective dual mTORC1 and mTORC2 inhibitors: the discovery of AZD8055 and AZD2014. *Bioorg Med Chem Lett* **23**(5): 1212–1216.

Prahallad A, Sun C, Huang S, Di Nicolantonio F, Salazar R, Zecchin D, Beijersbergen RL, Bardelli A, Bernards R (2012) Unresponsiveness of colon cancer to BRAF(V600E) inhibition through feedback activation of EGFR. *Nature* **483**(7387): 100–103.

Rajurkar M, Dang K, Fernandez-Barrena MG, Liu X, Fernandez-Zapico ME, Lewis BC, Mao J (2017) IKBKE is required during KRAS-induced pancreatic tumorigenesis. *Cancer Res* **77**(2): 320–329.

Raymond CS, Soriano P (2010) ROSA26Flpo deleter mice promote efficient inversion of conditional gene traps in vivo. *Genesis* **48**(10): 603–606.

Renshaw J, Taylor KR, Bishop R, Valenti M, De Haven Brandon A, Gowan S, Eccles SA, Ruddle RR, Johnson LD, Raynaud FI, Selfe JL, Thway K, Pietsch T, Pearson AD, Shipley J (2013) Dual blockade of the PI3K/AKT/mTOR (AZD8055) and RAS/MEK/ERK (AZD6244) pathways synergistically inhibits rhabdomyosarcoma cell growth *in vitro* and *in vivo*. *Clin Cancer Res* **19**(21): 5940–5951.

Rozengurt E, Soares HP, Sinnet-Smith J (2014) Suppression of feedback loops mediated by PI3K/mTOR induces multiple overactivation of compensatory pathways: an unintended consequence leading to drug resistance. *Mol Cancer Ther* **13**(11): 2477–2488.

Saxton RA, Sabatini DM (2017) mTOR signaling in growth, metabolism, and disease. *Cell* **168**(6): 960–976.

Schneeweis C, Wirth M, Saur D, Reichert M, Schneider G (2016) Oncogenic KRAS and the EGFR loop in pancreatic carcinogenesis – a connection to licensing nodes. *Small GTPases* **23**: 1–8.

Schneider G, Schmidt-Supprian M, Rad R, Saur D (2017) Tissue-specific tumorigenesis: context matters. *Nat Rev Cancer* **17**(4): 239–253.

Schonhuber N, Seidler B, Schuck K, Veltkamp C, Schachtler C, Zukowska M, Eser S, Feyerabend TB, Paul MC, Eser P, Klein S, Lowy AM, Banerjee R, Yang F, Lee CL, Moding EJ, Kirsch DG, Scheideler A, Alessi DR, Varela I, Bradley A, Kind A, Schnieke AE, Rodewald HR, Rad R, Schmid RM, Schneider G, Saur D (2014) A next-generation dual-recombinase system for time- and host-specific targeting of pancreatic cancer. *Nat Med* **20**(11): 1340–1347.

Subramanian A, Tamayo P, Mootha VK, Mukherjee S, Ebert BL, Gillette MA, Paulovich A, Pomeroy SL, Golub TR, Lander ES, Mesirov JP (2005) Gene set enrichment analysis: a knowledge-based approach for interpreting genome-wide expression profiles. *Proc Natl Acad Sci USA* **102**(43): 15545–15550.

von Burstin J, Eser S, Paul MC, Seidler B, Brandl M, Messer M, von Werder A, Schmidt A, Mages J, Pagel P, Schnieke A, Schmid RM, Schneider G, Saur D (2009) E-cadherin regulates metastasis of pancreatic cancer *in vivo* and is suppressed by a SNAIL/HDAC1/HDAC2 repressor complex. *Gastroenterology* **137**(1): 361–371 e1–5.

Wei F, Zhang Y, Geng L, Zhang P, Wang G, Liu Y (2015) mTOR inhibition induces EGFR feedback activation in association with its resistance to human pancreatic cancer. *Int J Mol Sci* **16**(2): 3267–3282.

Wirth M, Stojanovic N, Christian J, Paul MC, Stauber RH, Schmid RM, Hacker G, Kramer OH, Saur D, Schneider G (2014) MYC and EGR1 synergize to trigger tumor cell death by controlling NOXA and BIM transcription upon treatment with the proteasome inhibitor bortezomib. *Nucleic Acids Res* **42**(16): 10433–10447.

Wu CY, Carpenter ES, Takeuchi KK, Halbrook CJ, Peverley LV, Bien H, Hall JC, DelGiorno KE, Pal D, Song Y, Shi C, Lin RZ, Crawford HC (2014) PI3K regulation of RAC1 is required for KRAS-induced pancreatic tumorigenesis in mice. *Gastroenterology* **147**(6): 1405–1416 e7.

Ying H, Kimmelman AC, Lyssiotis CA, Hua S, Chu GC, Fletcher-Sananikone E, Locasale JW, Son J, Zhang H, Coloff JL, Yan H, Wang W, Chen S, Viale A, Zheng H, Paik JH, Lim C, Guimaraes AR, Martin ES, Chang J, Hezel AF, Perry SR, Hu J, Gan B, Xiao Y, Asara JM, Weissleder R, Wang YA, Chin L, Cantley LC, DePinho RA (2012) Oncogenic Kras maintains pancreatic tumors through regulation of anabolic glucose metabolism. *Cell* **149**(3): 656–670.

Yoshida T, Zhang G, Smith MA, Lopez AS, Bai Y, Li J, Fang B, Koomen J, Rawal B, Fisher KJ, Chen YA, Kitano M, Morita Y, Yamaguchi H, Shibata K, Okabe T, Okamoto I, Nakagawa K, Haura EB (2014) Tyrosine phosphoproteomics identifies both codrivers and cotargeting strategies for T790M-related EGFR-TKI resistance in non-small cell lung cancer. *Clin Cancer Res* **20**(15): 4059–4074.

Zhuang G, Yu K, Jiang Z, Chung A, Yao J, Ha C, Toy K, Soriano R, Haley B, Blackwood E, Sampath D, Bais C, Lill JR, Ferrara N (2013) Phosphoproteomic analysis implicates the mTORC2-FoxO1 axis in VEGF signaling and feedback activation of receptor tyrosine kinases. *Sci Signal* **6**(271): ra25.

Supplementary Information accompanies this paper on British Journal of Cancer website (http://www.nature.com/bjc)